Boundary-Layer Meteorol (2016) 161:145–163
DOI 10.1007/s10546-016-0159-4

RESEARCH ARTICLE

The Formation of Barrier Winds East of the Loess Plateau and Their Effects on Dispersion Conditions in the North China Plains

Xiao-Ming Hu[1,2] · Xingliang Li[3,4] · Ming Xue[2] · Dui Wu[5] · Jose D. Fuentes[6]

Received: 25 September 2015 / Accepted: 5 April 2016 / Published online: 18 April 2016

Abstract The North China Plain (NCP) to the east of the Loess Plateau is one of the most heavily polluted areas in the world. Weak surface flow in the western part of the NCP exacerbates the air pollution in this region. Deceleration of low-level flow when approaching the Loess Plateau, together with enhanced roughness associated with large cities, were previously ascribed as the causes for low wind speeds in the NCP. Using numerical simulations with a one-layer dispersion model, we identify that dynamic modification of airflow by the Loess Plateau (not just simple deceleration due to mountain blocking) plays an important role in reducing the wind speed over the NCP. Dynamically-induced northerly barrier winds, superimposed on the prevailing southerly/south-easterly flow, reduce the wind speed in a 50–100 km wide region to the east of the Plateau, partially explaining the weak winds in the western part of the NCP. Poor dispersion conditions due to weak horizontal winds likely contribute to the accumulation of pollutants in this region.

Keywords Air pollution · Barrier wind · Dynamic modification process · One-layer slab model

✉ Xiao-Ming Hu
xhu@ou.edu

Xingliang Li
lixl@cams.cma.gov.cn

1 Nanjing University of Information Science and Technology, Nanjing 210044, China

2 Center for Analysis and Prediction of Storms, and School of Meteorology, University of Oklahoma, Norman, OK 73072, USA

3 National Meteorological Center, China Meteorological Administration, Beijing 100081, China

4 Center for Analysis and Prediction of Storms, University of Oklahoma, Norman, OK 73071, USA

5 Institute of Technology on Atmospheric Environmental Safety and Pollution Control, Jinan University, Guangzhou 510632, China

6 Department of Meteorology, Pennsylvania State University, University Park, PA 16802, USA

1 Introduction

Due to extensive industrialization and urbanization in the past few decades, the North China Plain (NCP) to the east of the Loess Plateau (see the locations and terrain heights in Fig. 1a) has become one of the most heavily polluted areas in the world (van Donkelaar et al. 2010; Quan et al. 2011; Ma et al. 2012b; Zhang et al. 2012b; Huang et al. 2014). Inside of the NCP, an east-to-west gradient of severity of air pollution has been identified (e.g., Qu et al. 2010; Wei et al. 2011b; Hu et al. 2014a; Wang et al. 2014a; Wu et al. 2014; Mao et al. 2016). The western part of the NCP has experienced frequent severe haze pollution since the 1970s (Wu et al. 2014; Fig. 1a) and most extreme concentrations of pollutants have been observed in this area (Wang et al. 2014a). The severe regional air pollution in the NCP has attracted extensive research attention, e.g., He et al. (2001), Ding et al. (2008), Lin et al. (2008), Xu et al. (2011b), Ma et al. (2012a), Chen et al. (2013b), Han et al. (2015). The NCP air pollution is due to multiple pollutants, including particulate matter, nitrogen oxides, sulfur dioxide, and carbon monoxide (Huang et al. 2013; Wang et al. 2014b; Zhang et al. 2015a). Power plants, domestic heating, industry, vehicle exhaust, livestock, and fertilizer application all contribute (Han et al. 2015; Zhao et al. 2013a). Chemical reactions and the formation of secondary pollutants downwind of the sources further complicate the situation.

Emissions alone (see Fig. 5 of Qu et al. 2010; Fig. 6 of Huang et al. 2013; Fig. 1 of Hu et al. 2014; Fig. 10 of Wei et al. 2011b) cannot explain the spatial preference of the pollution in the NCP, even assuming a steady (homogeneous) boundary-layer wind field (Wang et al. 2014a; Ye et al. 2015). Analyses (Wei et al. 2011b) indicate that the spatial distribution of ambient pollutants and emissions over the NCP are not consistent. In addition to direct emissions, meteorological conditions also play an important role in modulating ambient concentrations of air pollutants in this region (Zhang et al. 2009a, b; Wang et al. 2010a, b; Gao et al. 2011; Wei et al. 2011a; Yang et al. 2011; Hu et al. 2014b; Ji et al. 2014; Quan et al. 2014; Zhang et al. 2015b). Southerly/south-easterly surface winds dominate in the NCP during most of the year (Xu et al. 2011a; Fu et al. 2014; Cao et al. 2015) and a climatological west-to-east gradient of wind speed persists (Fig. 1b). This wind pattern is most prominent in summer, when a subtropical anticyclone persists to the south-east of the NCP, although it is also common in spring (Fig. 2). The southerly winds are more likely associated with severe air pollution in the NCP than is the case for other wind directions (Chen et al. 2008; Meng et al. 2009; Wang et al. 2010a; Zhang et al. 2012a; Lang et al. 2013; Wang et al. 2013; Feng et al. 2014; Jiang et al. 2015). Low surface wind speeds in the western part of the NCP were found to play an important role in exacerbating the air pollution in this region (Sun et al. 2006; An et al. 2007; Wu et al. 2008; Xu et al. 2011b; Zhao et al. 2013b; Fu et al. 2014; Wang et al. 2014a; Zhang et al. 2014; Chen and Wang 2015; Xu et al. 2015; Ye et al. 2015). Flow deceleration on approach to the Loess Plateau, together with enhanced surface roughness associated with large cities, was reported to cause the reduction in wind speed in the NCP (Fu et al. 2014; Wang et al. 2014a; Cao et al. 2015). Hu et al. (2016), however, demonstrated that a reduction in wind speed due to the presence of the urban area is highly confined to the central urban area. Thus, urban friction cannot explain the reduction in boundary-layer wind speed in a region as large as the NCP. In this study we explore whether other dynamic modifications of the wind field by the Loess Plateau (not just the simple deceleration due to mountain blocking) play an important role in reducing the wind speed over the NCP.

Dynamic modification of the large-scale wind field by mountainous terrain [called 'passive effects of mountains' by De Wekker and Kossmann (2015)] manifests itself in different

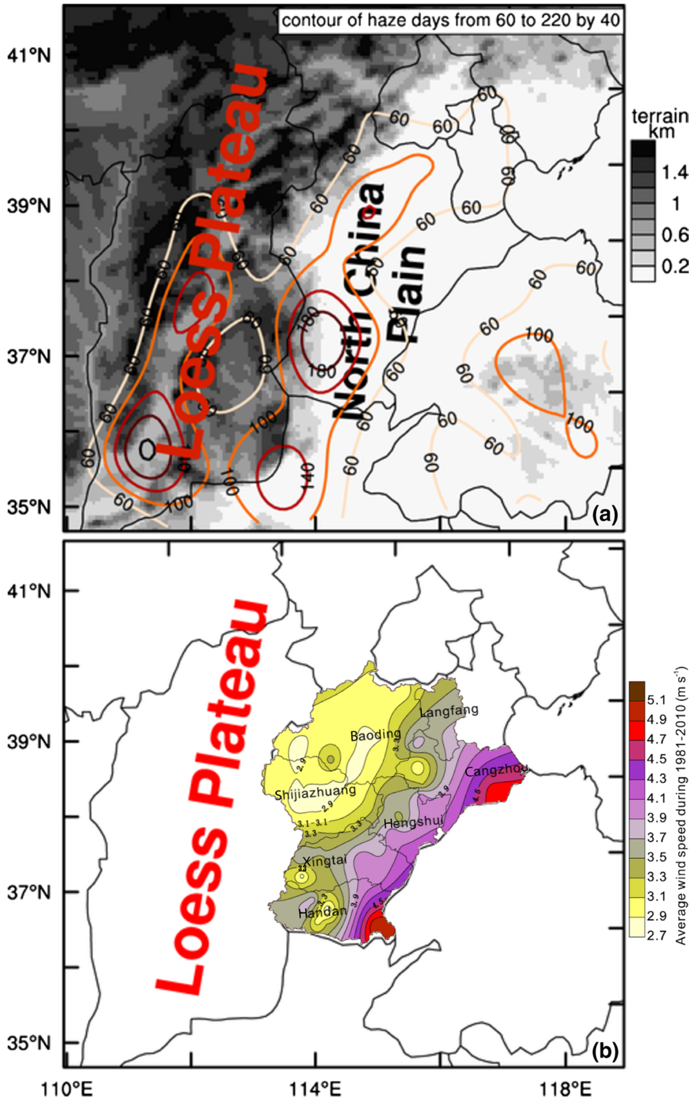

Fig. 1 **a** Distribution of annual number of haze days (contour lines) between 2001 and 2005 [adapted from Fig. 2 of Wu et al. 2014] overlaid on orography (*gray shade*) around the North China Plain (NCP); **b** distribution of average 10-m wind speed at 1400 local time during 1981–2010 in the southern NCP [adapted from Fig. 6a of Fu et al. (2014)]

atmospheric flow phenomena, including flow over and around mountains (Malkus 1955; Smith 1982; Pierrehumbert and Wyman 1985; Chen and Feng 2001; Hu and Liu 2005; Yang and Chen 2008), airflow channelling in valleys (Whiteman and Doran 1993; Hitzl et al. 2014), flow separation (Vosper et al. 2006; Sheridan et al. 2007) and barrier winds (Schwerdtfeger 1979; Parish 1982; McCauley and Sturman 1999). In addition to affecting meteorological phenomena such as waves (Grubisic et al. 2008; Armi and Mayr 2011) and precipitation (Rotunno and Ferretti 2001; Chen et al. 2013a; Lee and Xue 2013), dynamic modification of the large-scale flow over mountainous regions plays an impor-

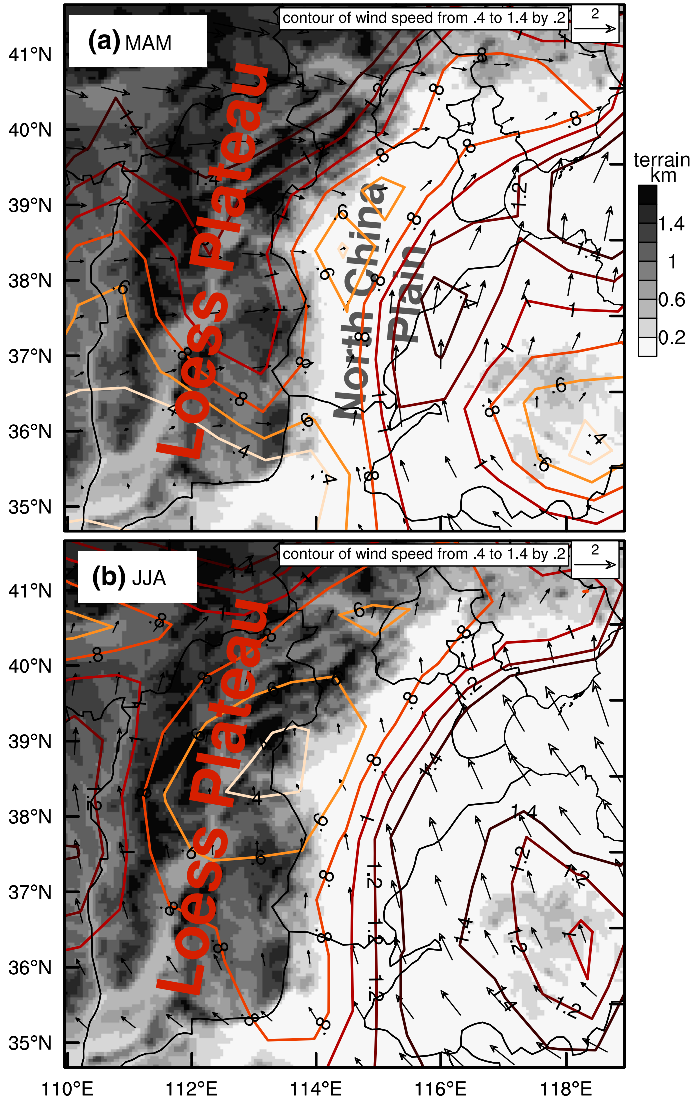

Fig. 2 Seasonal mean wind fields during 1981–2010 at 1000 hPa in **a** spring (March, April, and May), and **b** summer (June, July, and August) derived from the European Centre for Medium-range Weather Forecasts (ECMWF) ERA-interim data

tant role in the transport and dispersion of air pollutants (Steyn et al. 2013; Emery et al. 2015).

Barrier winds occur when flow approaches an extra-tropical barrier (such as a mountain or plateau) and is blocked by the barrier for time scales of hours or longer (long enough for the Coriolis force to exert an influence) (Jackson et al. 2013). In the Northern (Southern) Hemisphere, the impinging flows turn to the left (right) along the barrier (i.e., cyclonic turning) in response to decreased Coriolis force as the blocked flows decelerate. The blocking of the flows creates a high-pressure region along the mountain barrier (Olson and Colle 2009;

Jackson et al. 2013), and as a result of the enhanced across-barrier pressure gradient and unbalanced mountain-parallel pressure gradient, a mountain-parallel barrier jet develops on the windward side of the mountains (Xu 1990; Jackson et al. 2013). The across-barrier blocking, turning, and acceleration of the flow (i.e., formation of barrier jets) have been reported in many regions (Schwerdtfeger 1975; Parish 1983; Overland and Bond 1993, 1995; Holt 1996; Doyle 1997; Li and Chen 1998; Colle et al. 2002; Loescher et al. 2006; Olson et al. 2007; Olson and Colle 2009; Harden et al. 2011; Jackson et al. 2013; Emery et al. 2015). In the case of flow with an easterly component impinging on a north-south oriented barrier, northerly/southerly barrier jets occur that advect any present cold air southward/northward in the Northern/Southern Hemisphere, creating a cold dome along the barrier. This subset of barrier jets is also termed cold-air damming (Bell and Bosart 1988; Xu 1990; Bailey et al. 2003; Petersen et al. 2009; Jackson et al. 2013; Colle 2015). In all the existing relevant research, the barrier winds, superimposed on the environmental wind field (i.e., the large-scale boundary-layer wind field without dynamic modification), lead to the formation of mountain-parallel jets. Here, we demonstrate that under certain circumstances barrier winds may lead to a decrease in environmental wind speed, for example in the NCP in the presence of a southerly/south-easterly prevailing flow.

As a necessary step to understanding the impact of meteorological factors (particularly the wind field) on air pollution in the NCP (Fu et al. 2014), we investigate the previously unrecognized development of barrier winds in the NCP and its impact on the spatial distribution of the wind field and the horizontal dispersion of pollutants in the NCP, using a one-layer dispersion model.

The article is organized as follows: in Sect. 2, development of the slab dispersion model and design of numerical experiments are described. In Sect. 3, the development of barrier winds and its impacts in the NCP are discussed using the model simulations. The manuscript concludes in Sect. 4 with a summary and discussions on the limitations of this study.

2 Methodology

A one-layer dispersion model based on a previously designed meteorological slab model (Lindzen and Nigam 1987; Pu and Dickinson 2014) is developed to examine the dynamic modification of the boundary-layer winds over the NCP by the Loess Plateau and the subsequent impact on the horizontal dispersion of pollutants, formulated as follows,

$$\frac{\partial u}{\partial t} = -u\frac{\partial u}{\partial x} - v\frac{\partial u}{\partial y} + fv - g\frac{\partial h}{\partial x} - \phi_x, \tag{1}$$

$$\frac{\partial v}{\partial t} = -u\frac{\partial v}{\partial x} - v\frac{\partial v}{\partial y} - fu - g\frac{\partial h}{\partial y} - \phi_y, \tag{2}$$

$$h = -\tau H\left(\frac{\partial u}{\partial x} + \frac{\partial v}{\partial y}\right), \tag{3}$$

$$\frac{\partial C}{\partial t} = -u\frac{\partial C}{\partial x} - v\frac{\partial C}{\partial y}, \tag{4}$$

where u and v are the zonal and meridional wind components, C is the puff concentration of a passive pollutant (with units of μg m^{-3}) emitted from the stacks within the domain, $f = 2\Omega\sin\varphi$ is the Coriolis parameter, $\Omega = 7.27 \times 10^{-5}\,\mathrm{s}^{-1}$ is the angular speed of rotation of the Earth, φ is latitude, and ϕ_x and ϕ_y are zonal and meridional geopotential gradients. As a slab model, the domain is defined for the air layer extending from the surface to some depth of the atmosphere ($H \approx 1$ km), assuming an atmospheric boundary layer with a strong capping inversion (Hu et al. 2014b; Miao et al. 2015); h is the perturbation height of the layer top, representing the pressure perturbation caused by mountain blocking and subsequent flow rising [called the interactive component of forcing in Pu and Dickinson (2014)]. We follow the assumption of Lindzen and Nigam (1987) that convergence (i.e., $-\left(\frac{\partial u}{\partial x} + \frac{\partial v}{\partial y}\right)$) in the boundary layer is taken up by the layer above in a short time (τ), thus $\tau = 20$ s is used.

A simplified version of the above slab model, not considering the pollutant and linearized by excluding the horizontal advection terms on the right-hand side of Eqs. 1 and 2 and adding an additional term representing surface frictional effect, was applied in Pu and Dickinson (2014) to reproduce the diurnal cycle of the Great Plains low-level jet and associated variation of convergence/vorticity. The slab model is modified here by including the advection terms to investigate the response of the prevailing southerly/south-easterly flow in the NCP to the dynamic modification by the Plateau. The advection process is critical to mimicking the continuous large-scale forcing by the prevailing flow in the NCP. Pollutant puffs emitted within the domain (indicated by C) are tracked using the advection equation (i.e., Eq. 4) to investigate the impact of horizontal flow on the dilution of pollutants emanating from emission sources. Puffs with constant amount of pollutant are allowed to be emitted from two stacks within the domain (see their locations in Fig. 3e) hourly (i.e., with a constant emission rate) from hour 12 to 16 (i.e., after the flow reaches equilibrium). The length of the plumes (composed of the puffs) dictates the total volume of air available for the pollutant transport and dispersion, thus indicating the dilution of the emitted pollutant.

Considering the south-north orientation (with a slight incline to the east) of the eastern edge of the Loess Plateau and the spatial coverage of the NCP (Fig. 1a), the slab model is configured for a square 400 km $\times$ 400 km domain covering the region of $36° - 40°$N and $114 - 118°$E, mimicking the core of the NCP. All simulations are conducted on an f plane ($\varphi = 38°$N), with time-independent geopotential gradients, i.e., constant ϕ_x and ϕ_y, prescribed as large-scale forcings (in a geostrophic balance with the environmental inflow). Since the large-scale forcings are set constant, the interactive component of forcing, i.e., h, dictates the final equilibrium wind field. A slip-wall boundary condition (i.e., $u = 0$) is set at the west boundary to mimic the blocking effect of the Loess Plateau. An open boundary condition (with a constant prevailing wind speed) is set at the east boundary to mimic the continuous forcing. A periodical boundary condition is set at the south and north boundaries.

Note that a vertical wall of 1-km depth is set on the west domain boundary for simplicity, while the real orography shows a slope (plateau height/windward slope width) of about 1:50 (figure not shown). Such a slope has been shown in Braun et al. (1999) to be steep enough to decelerate incident flows, and to generate sufficient convergence and pressure perturbations to lead to barrier-jet formation on the windward side of a westward-facing plateau.

The slab model is numerically solved using the centre finite difference method on the staggered Arakawa C grid in space (Arakawa and Lamb 1977) with a 1 km $\times$ 1 km horizontal grid spacing. Equations 1, 2, and 4 are integrated in time using the second-order total variation diminishing Runge-Kutta method (Gottlieb and Shu 1998; Xue and Lin 2001; Li et al. 2013), which helps improve the numerical accuracy and stability. The model was integrated with a timestep of 1 s for 16 h (longer than the time needed to reach equilibrium). The complete model configuration mentioned above is referred to as the base configuration. Considering the prevailing southerly/south-easterly wind direction (Fu et al. 2014; Fig. 2) and the orientation of the mountains (Fig. 1a), an environmental wind speed of 6 m s^{-1} and a direction of 150° are set in the control simulation with the base configuration.

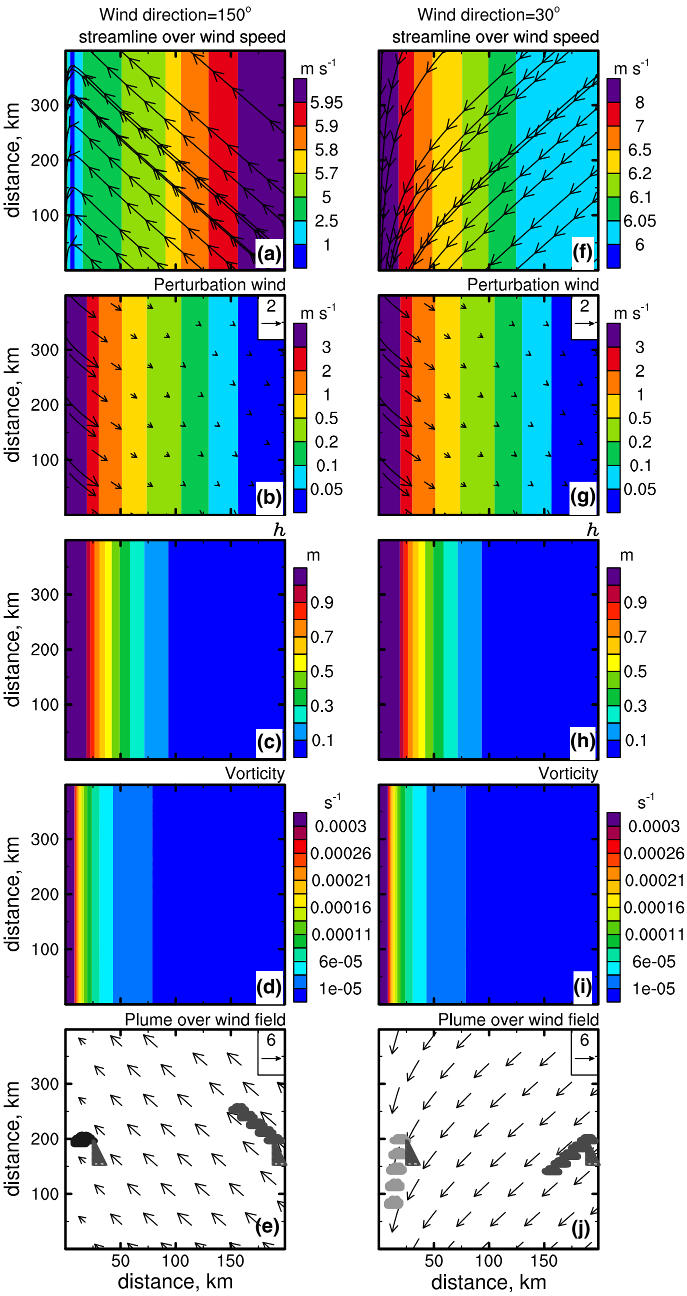

Fig. 3 Spatial distribution of simulated **a**, **f** wind speed with streamlines overlaid on *top*, **b**, **g** perturbation wind (i.e., wind-inflow), **c**, **h** interactive forcing (h), **d**, **i** vorticity at hour =12 (when the fields reach equilibrium), and **e**, **j** dispersion of pollutant puffs from two stacks at hour =16 in the presence of an environment wind (i.e., inflow) with speed of 6 m s^{-1} and directions of (*left*) 150° and (*right*) 30°. *Two triangles* in panels e, j indicate the location of the stacks. Note the simulation domain is 400 km × 400 km, the resultant equilibrium fields on the *right side* of the domain are dictated by the inflow from the right boundary and barely impacted by the *left* boundary. Thus only the 200 km wide domain near the *left* boundary (where is affected by the mountain blocking) is shown in each *panel*

Table 1 Details of the two configurations of the simulations conducted in this study with the slab dispersion model

Configurations	Details
Base	Described in Eqs. 1–4
CONF_S1	Maintain the Coriolis force of the background environmental flow homogenously constant over the whole simulation domain, thus setting to zero the Coriolis force of the barrier flow

Sensitivity simulations with the base configuration are conducted to examine the effect of large-scale forcing and ambient wind directions (or impinging angles) by varying the incoming wind speed within a plausible wind-speed range, from 3 to 9 m s^{-1} at an incremental step of 3 m s^{-1}, and varying the incoming wind direction from 015° to 165° from north at 15° intervals. Previous studies (e.g., Barstad and Gronas 2005; Olson and Colle 2009) examined the sensitivity of barrier jets to the ambient wind direction, but ambient winds were limited to one sector of nearly terrain-parallel to nearly terrain-perpendicular, i.e., the impinging angle $<90°$. Our study extends previous investigations to illustrate the different dynamic impacts when ambient winds impinge upon the mountains at all possible angles (between 0 and 180°).

To quantify the contribution of the simple deceleration by mountain blocking to the reduction in wind speed, the slab model is run with another configuration (i.e., CONF_S1 in Table 1), in which the Coriolis force due to the perturbation wind (i.e., the difference between the actual wind and the inflow wind) is not considered, that is, the geostrophic adjustment processes associated with the flow change is ignored. Thus the final reduction in wind speed is simply due to deceleration by mountain blocking.

Since the model only simulates one layer of dry air, a few simplifications are applied here, including (1) simplification of the orography, (2) neglect of land-surface processes, thermally induced effects (e.g., stability change, thermotopographic winds), and possible influences from high-level jet streaks, and (3) omission of humidity and clouds, as in Pu and Dickinson (2014). In terms of pollutants, only horizontal advection is considered, and chemical processes that affect emission, conversion, decay and deposition of pollutants are omitted. Previous numerical sensitivity experiments designed to examine mountain effects (e.g., Cui et al. 1998; Barstad and Gronas 2005; Hu et al. 2014b; Nielsen et al. 2016) considered both dynamic and thermal effects of mountainous terrain. Particularly, in our previous studies (i.e., Hu et al. 2014b; Hu and Xue 2016), three-dimensional (3-D) WRF simulations were conducted. Since all the effects were simultaneously considered in the 3-D simulations, the dynamic and thermal effects could not be easily separated. In contrast, in this study we ignore the thermal effect and apply other simplifications to isolate the dynamic effect of the mountain barrier on the low-level wind field, and the subsequent impact on the horizontal dilution of pollutants. Using such an idealized approach helps us better understand the complex contributions of various effects/processes to the near-surface wind pattern and pollution (Braun et al. 1999; Saide et al. 2011; Pu and Dickinson 2014).

3 Results

3.1 Barrier-Wind Formation and Its Impact on the Spatial Distribution of Wind Fields

In the control simulations, an environmental inflow with wind speed of 6 m s^{-1} and direction of 150° enters the domain from the eastern boundary, mimicking a climatological southerly/south-easterly flow impinging upon the slightly inclined south-to-north oriented mountains of the Loess Plateau. The wind field (Fig. 3a) reaches equilibrium after about 10 h of numerical simulation as suggested by the evolution of h, an indicator of pressure perturbation (figure not shown). Our primary interest here is in the steady-state wind field under the influence of dynamic modification due to the mountain barrier. Thus our analysis in terms of the wind field focuses on the steady state at 12 h of simulation.

The environmental inflow approaches the mountain barrier on the left domain boundary and is blocked by the barrier (Fig. 3a). As reported by many previous studies (Wang et al. 2010a, 2014a), convergence occurs near the barrier, which is taken up by the upper layer as described in Eq. 3, thus creating a higher pressure perturbation along the barrier (Fig. 3c). The pressure perturbation caused by mountain blocking leads to the formation of the barrier wind. Here we define the barrier wind as the perturbation wind caused by mountain blocking, i.e., the difference between the equilibrium wind and the inflow wind. Geostrophic adjustment turns the barrier wind to the right with time (Fig. 3b), so that high pressure is to the right. The equilibrium barrier wind is in almost the opposite direction of the ambient environmental flow. Thus, superimposed on the environmental flow, the formation of the barrier wind considerably reduced the wind speed near the mountain barrier.

The dynamic modification (or barrier-wind formation) process can be interpreted in another way. As the ambient flow approaches the mountain, it decelerates in the across-barrier direction, resulting in a weakened Coriolis force. In the along-barrier direction, the large-scale south-to-north pressure gradient remains and acts to decelerate the northward movement of the ambient flow.

As the result of the dynamic modification (i.e., barrier-wind formation), a wind minimum band develops near the barrier, with the wind reduction greater where it is closer to the barrier. In the 100-km wide band near the barrier the ambient wind speed is reduced by at least 0.2 m s^{-1} (3 %), while in the 50-km wide band near the barrier the ambient wind speed is reduced by at least 1 m s^{-1} (17 %) (Fig. 3a). The horizontal extent of the barrier wind is consistent with previous studies (Parish 1982; Jackson et al. 2013). The resulting west-to-east gradient of wind speed (Fig. 3a) is quite similar to both the climatological distribution of wind speed over the NCP (Fig. 1b) derived in Fu et al. (2014), in which the 10-m wind speed at 50 km from the plateau is lower than that 200 km from the plateau by about 17 % (3.3 vs. 4 m s^{-1}), and to the seasonal mean gradient of near-surface wind in spring and summer during the past three decades (i.e., 1981–2010) derived from the European Centre for Medium-range Weather Forecasts (ECMWF) ERA-interim data (Fig. 2). Thus our numerical experiment illustrates that barrier-wind formation is a key factor in explaining the spatial distribution of the wind field in the NCP. Note that in winter, due to different large-scale forcing and frequent disturbances by transient processes (e.g., fronts, troughs), the seasonal mean wind direction in the NCP is north-westerly (Miao et al. 2015), which is not considered herein. We only consider the wind with an easterly component, i.e., impinging on the Loess Plateau; this does not mean that the barrier-wind formation mechanism does not apply in winter. Figure 3a illustrates that as long as the background environmental flow is south-easterly on winter days, the west-to-east gradient of wind speed could occur in the NCP.

Previous studies of barrier winds all reported low-level barrier-parallel jets on the windward side of mountains (Jackson et al. 2013). The above experiment illustrates that barrier-wind formation, instead of leading to jets, may reduce the ambient wind speed. The impinging angle of the inflow is hypothesized to be responsible for the difference. Thus, a sensitivity simulation with an environmental wind speed of 6 m s^{-1} and a wind direction of 30° is conducted. In this case, a barrier-parallel jet indeed forms along the mountain barrier (Fig. 3f). As with the control case, a higher pressure perturbation forms along the barrier when the inflow impinges upon the barrier, and the resulting barrier wind is adjusted by the Coriolis force and turns to the right (Fig. 3g). Superimposed on the north-easterly ambient flow, the formation of the barrier wind turns the ambient wind cyclonically and leads to barrier-jet formation on the windward side of the mountain (Fig. 3f).

The cyclonic turning of the flow can also be explained in terms of the vorticity budget. Taking $\partial/\partial x$ of Eq. 2 and subtracting $\partial/\partial y$ of Eq. 1 gives the rate of relative vorticity,

$$\frac{\partial \zeta}{\partial t} = -u\frac{\partial \zeta}{\partial x} - v\frac{\partial \zeta}{\partial y} - (\zeta + f)\left(\frac{\partial u}{\partial x} + \frac{\partial v}{\partial y}\right), \tag{5}$$

on an f plane, where $\zeta = \partial v/\partial x - \partial u/\partial y$ is relative vorticity. The first two terms on the right-hand side represent advection of relative vorticity, and the last term on the right-hand side represents the effect of horizontal convergence on vorticity. When the flow approaches the mountain barrier (Fig. 3a, f), convergence occurs (Fig. 3c, h). According to the last term of Eq. 5, the convergence leads to an increase in the vorticity (Fig. 3d, i). A spatial analysis of vorticity fields in the NCP by Cao et al. (2015) also confirmed the enhanced vorticity in the west side of the NCP when the flow is blocked by the Plateau (their Fig. 5b). The increase in vorticity explains the cyclonic turning of the ambient flow after blockage by the mountain barrier.

The equilibrium barrier wind in the sensitivity simulation (Fig. 3g) is the same as that in the control simulation (Fig. 3b) as both ambient flows impinge upon the mountain barrier at a 30° angle from the mountain barrier, except that one is from the south-east (Fig. 3a) and one is from the north-east sector (Fig. 3f). Even though barrier winds are the same, different spatial distributions of wind speed are produced, i.e., a wind minimum band (Fig. 3a) vs. a jet (Fig. 3f), when the inflow directions are different, because the perturbation barrier winds are in the opposite and same direction as the ambient winds, respectively.

Additional sensitivity simulations were conducted to examine the responses of different plausible ambient flows to the dynamic modification of mountain barrier (Fig. 4). When the inflow wind speed is 3 m s^{-1}, a north-easterly flow leads to barrier jets (wind speed in the 50-km wide area near the barrier is enhanced by 56 and 49 % for 30° and 60° respectively, Table 2) and a south-easterly flow leads to wind minimum bands near the barrier (wind speed in the 50-km wide area is reduced by 22 and 48 % for 120° and 150° respectively, Table 2). The barrier-jet width tends to be narrow when the impinging flow is more perpendicular to the barrier, which is consistent with Olson and Colle (2009). In the case of an easterly wind direction, a narrow jet (about 10 km wide) develops near the barrier; beyond the narrow jet, a wide wind minimum band develops as a result of the deceleration in the across-barrier direction. When the ambient wind speed is higher, i.e., at 9 m s^{-1}, wind minimum bands still persist for the south-easterly wind (wind speed in the 50-km wide area is reduced by 44 and 39 % for 120° and 150° respectively, Table 2) and barrier jets also develop when the north-easterly wind impinges upon the barrier at low angles (wind speed in the 50-km wide area is enhanced by 23 % for 30°, Table 2). However, the barrier jets disappear when the north-easterly flow is more nearly perpendicular to the barrier, presumably due to substantial deceleration in the across-barrier direction. The different jet characteristics associated with different north-easterly ambient wind speeds suggest that the greatest wind-speed enhancements due to barrier-wind formation occur normally for relatively low wind speeds. Such a conclusion has also been suggested by Jackson et al. (2013).

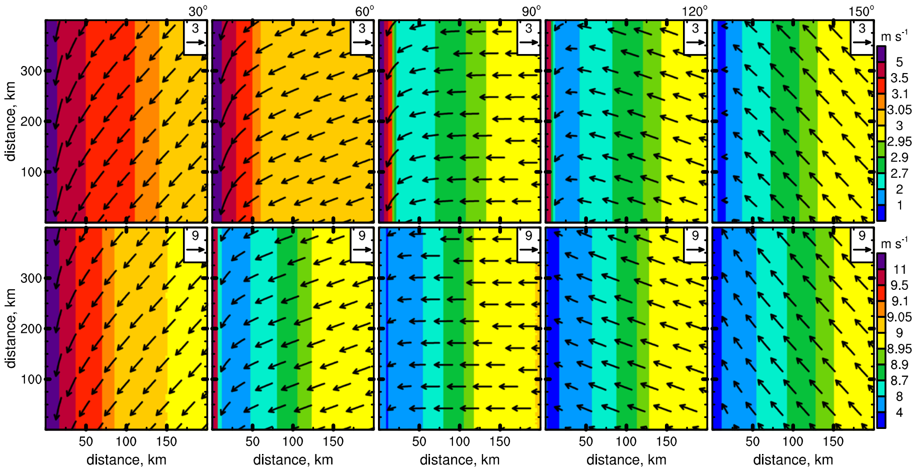

Fig. 4 Simulated equilibrium wind fields in the presence of environment winds with speed of (*top*) 3 and (*bottom*) 9 m s^{-1}, and direction of (*left* to *right*) 30°, 60°, 90°, 120°, and 150°

Table 2 Simulated average wind speed ($\bar{V}$) in the 50-km wide area near the barrier and the ratio of $\bar{V}$ to the background environmental $\bar{V}$ for all the cases with different environmental $\bar{V}$ and wind directions

	Average $\bar{V}$ (m s^{-1})					Ratio				
	north-easterly			south-easterly		north-easterly			south-easterly	
direction / speed	30	60	90	120	150	30	60	90	120	150
3	4.67	4.47	3.46	2.34	1.56	1.56	1.49	1.15	0.78	0.52
6	8.17	6.69	4.66	3.44	3.32	1.36	1.12	0.78	0.57	0.55
9	11.08	8.33	5.9	5.04	5.52	1.23	0.93	0.66	0.56	0.61

3.2 Contribution from the Simple Deceleration by Mountain Blocking

The above analysis illustrates that mountain blocking and the Coriolis force both play roles in the barrier-wind formation in the NCP, leading to a barrier jet in the presence of north-easterly environmental wind and a wind minimum band in the presence of south-easterly wind direction. A question arises as to how much contribution to the reduction of wind speed in the NCP arises from simple deceleration by mountain blocking, ignoring the Coriolis effect. Simulations with configuration CONF_S1 (Table 1) are conducted to isolate such a contribution. In such simulations when the Coriolis force associated with the perturbation wind is set to zero, the eastward perturbation wind does not turn to the right (Fig. 5b, d). Thus mountain blocking leads to the same wind reductions in both the north-easterly and south-easterly wind directions, with a wind speed of 5.3 m s^{-1} in the 50-km wide area near the barrier (Fig. 5a,c), representing a 12 % reduction from the environmental wind speed (6 m s^{-1}). Note that in the simulations with the base configuration (where the Coriolis force of the perturbation wind is considered), the barrier-wind formation leads to a 45 % reduction in wind speed near the barrier for the 150° wind, and a 36 % increase in wind speed for the 30° wind direction (Table 2). The comparison between the simulations with the base and CONF_S1 configurations confirms the importance of barrier-wind formation in the presence of the Coriolis force in explaining the wind distributions in the NCP.

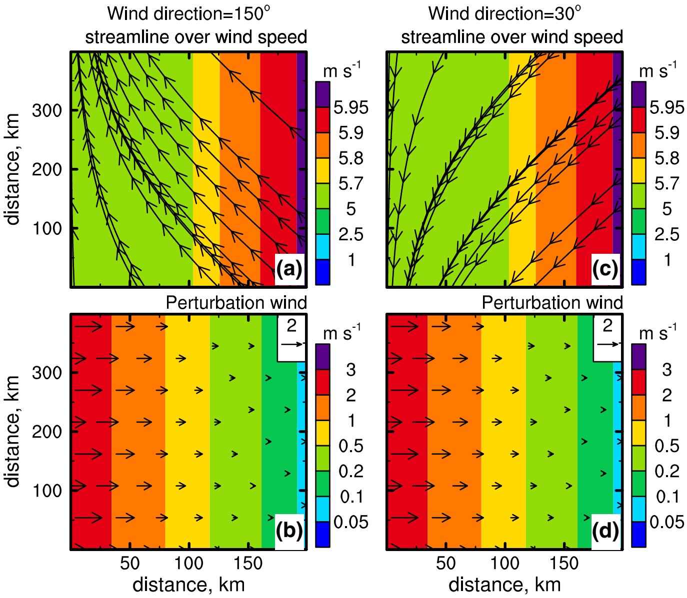

Fig. 5 **a**, **c** Wind speed with streamlines overlaid on *top*, **b**, **d** perturbation wind (i.e., wind-inflow) in the presence of environment flow with wind of 6 m s^{-1}, and direction of (*left*) 150° and (*right*) 30° simulated with the configuration of CONF_S1 (Table 1, i.e., turning off Coriolis force of the perturbation wind)

3.3 Implications for Dispersion of Pollutants

Wind fields dictate the dispersion and dilution of a pollutant after it has been emitted. Assuming the atmospheric residence time is long enough, the ambient concentration of directly emitted primary pollutants is approximately inversely proportional to the wind speed, i.e., the greater the wind speed the lower the concentration (Whiteman 2000; Schnadt and Ivanov 2012). In the case of the incident wind direction of 150°, the wind speed near the barrier is as low as about 1 m s^{-1} due to the northerly barrier-wind formation (Fig. 3a); while in case of the incident wind direction of 30°, the wind speed near the barrier is about 8 m s^{-1} (Fig. 3f). Thus the ambient concentration of the pollutant emitted near the barrier in the case of 30° incident flow is approximately eight times more diluted compared to the 150° case. Figure 3e,j shows the plumes at hour 16, which are composed of pollutant puffs emitted hourly between hours 12 and 16. The length of the plumes clearly demonstrates that the dispersion conditions become worse/better when the barrier is approached by a flow from the 150°/30°. Note that in cases where the barrier wind enhances the ambient wind speed (e.g., when the inflow is incident at 30°), greater wind speeds near the barrier also produce stronger shear-induced turbulence (Stull 1988), which diffuses the plume to a greater degree.

Such an impact of horizontal flow on dispersion of pollutants must play a role in modulating the air quality over the NCP. In the presence of the prevailing southerly/south-easterly winds, the northerly barrier-wind formation reduces the wind speed in the western part of the NCP, creating poor dispersion conditions, which contributes to the accumulation of pollutants in this region.

4 Conclusions and Discussion

Previous studies (e.g., Wei et al. 2011b) suggest that assuming a steady (homogeneous) boundary-layer wind field cannot explain the observed spatial distribution of pollutant concentrations in the North China Plain (NCP) given the known emission sources. The correlation between the spatial distributions of the annual number of haze days and wind speed in the NCP (Fig. 1) confirms that weak surface winds in the western part of the NCP play an important role in exacerbating the ambient air pollution in this region. The dynamic modification of wind fields in the NCP by the Loess Plateau is investigated using a one-layer slab model, which ignores the thermal effects of mountainous terrain and diabatic atmospheric processes, and thus can isolate the dynamic effect of the plateau barrier on the low-level wind field. The simulation results show that when ambient flow impinges upon the plateau barrier, a high pressure perturbation is created along the windward side of the barrier, resulting in barrier-wind formation. Geostrophic adjustment by the Coriolis force turns the barrier wind (i.e., the perturbation wind) to the right, i.e., the northerly component of the barrier wind increases with time until it reaches a geostrophic balance. Even though the barrier-wind formation mechanism is the same, depending on the ambient wind fields the barrier-wind formation leads to different spatial distributions of total wind speed. Superimposed on the north-easterly ambient flow with a moderate to low wind speed and a low impinging angle, the northerly barrier wind leads to the formation of a barrier jet on the windward side of the barrier. Such a scenario is similar to the classic barrier jets and the dynamic processes associated with cold-air damming events reported in many previous studies. Superimposed on the prevailing south-easterly wind, the northerly barrier wind reduces the wind speed in a 50–100 km wide region east of the plateau, creating weak surface winds consistent with observations in the western part of the NCP under such a situation. The barrier-wind formation mechanism provides a more complete theory than the simple deceleration by mountain blocking to explain the spatial distribution of wind speed in the NCP.

Barrier-wind formation has been widely studied around the world, with a reported low-level barrier-parallel jet (below mountain height) on the windward side of the mountains. Our study demonstrates that, instead of increasing the ambient wind speed, barrier-wind formation may reduce the ambient wind speed in certain circumstances.

Deceleration of the ambient flow when approaching the Loess Plateau, together with enhanced roughness associated with large cities, were ascribed as the causes for the low wind speed in the NCP in previous studies (Fu et al. 2014; Wang et al. 2014a). Our study reveals that northerly barrier-wind formation plays a role in reducing the speed of the prevailing southerly/south-easterly flow over the NCP, which suppresses the dispersion of pollutants. Such poor dispersion conditions must partially contribute to the frequent accumulation of pollutants in the western part of the NCP (Fig. 1a). Under such circumstances, increased efforts may be required to control emissions in order to prevent air pollution episodes in the NCP. On the other hand, barrier-jet formation in the presence of flow with a north-easterly component leads to good dispersion conditions. Our new findings regarding the causes for the spatial distribution of wind fields in the NCP thus have important implications for better identifying the essential meteorological factors for pollution episodes, and for forecasting air pollution in this region.

Although the dynamic effect of the Loess Plateau and its implications for dispersion condition have been emphasized, the thermal effects of the Plateau (e.g., convection, mountain-valley wind systems) cannot be deemphasized when considering implications on air quality close to the mountains (De Wekker 2008; Steyn et al. 2013; De Wekker and

Kossmann 2015; Rendon et al. 2015). Our previous 3D simulations (Hu et al. 2014b; Miao et al. 2015) reveal that the mountain-plain breeze circulation induced by the thermal contrast between the Loess Plateau and the NCP is most prominent in autumn and summer. Such a thermal process suppresses boundary-layer development over the NCP and enhances the air pollution. The dispersion model developed here ignores the thermal effects and does not account for variations in boundary-layer height and turbulent mixing, which is a significant limitation. Nevertheless, we have identified the previously unrecognized development of barrier winds in the NCP and their impact on pollutant dispersion, which is a necessary/critical initial step for future investigations of those dynamic and thermal processes and their interactions, as well as their impacts on air quality (Emery et al. 2015)

Acknowledgments This work was supported by the National Natural Science Foundation of China (Nos. 41375108; 41375109) and by a Ministry of Science and Technology of China ‘973’ Project (2013CB430103). Proofreading by Charlotte E. Wainwright is greatly appreciated. Three anonymous reviewers provided helpful comments that improved the manuscript.

References

An X, Zhu T, Wang Z, Li C, Wang Y (2007) A modeling analysis of a heavy air pollution episode occurred in Beijing. Atmos Chem Phys 7:3103–3114

Arakawa A, Lamb VR (1977) Computational design of the basic dynamical processes of the UCLA general circulation model. In: Julius C (ed) Methods in computational physics: advances in research and applications, vol 17. Elsevier, Amsterdam, pp 173–265. doi:10.1016/B978-0-12-460817-7.50009-4

Armi L, Mayr GJ (2011) The descending stratified flow and internal hydraulic jump in the Lee of the Sierras. J Appl Meteorol Clim 50:1995–2011. doi:10.1175/Jamc-D-10-05005.1

Bailey CM, Hartfield G, Lackmann GM, Keeter K, Sharp S (2003) An objective climatology, classification scheme, and assessment of sensible weather impacts for Appalachian cold-air damming. Weather Forecast 18:641–661. doi:10.1175/1520-0434(2003)018

Barstad I, Gronas S (2005) Southwesterly flows over southern Norway—mesoscale sensitivity to large-scale wind direction and speed. Tellus A 57:136–152. doi:10.1111/j.1600-0870.2005.00112.x

Bell GD, Bosart LF (1988) Appalachian cold-air damming. Mon Weather Rev 116:137–161. doi:10.1175/1520-0493(1988)116

Braun SA, Rotunno R, Klemp JB (1999) Effects of coastal orography on landfalling cold fronts. Part I: dry, inviscid dynamics. J Atmos Sci 56:517–533. doi:10.1175/1520-0469(1999)056

Cao Z, Sheng L, Liu Q, Yao X, Wang W (2015) Interannual increase of regional haze-fog in North China Plain in summer by intensified easterly winds and orographic forcing. Atmos Environ 122:154–162. doi:10.1016/j.atmosenv.2015.09.042

Chen CY, Chen YL, Chen CS, Lin PL, Liu CL (2013) Revisiting the heavy rainfall event over Northern Taiwan on 3 June 1984. Terr Atmos Ocean Sci 24:999–1020. doi:10.3319/Tao.2013.07.04.01(a)

Chen H, Wang H (2015) Haze days in North China and the associated atmospheric circulations based on daily visibility data from 1960 to 2012. J Geophys Res. doi:10.1002/2015JD023225

Chen PF, Quan JN, Zhang Q, Tie XX, Gao Y, Li X, Huang MY (2013) Measurements of vertical and horizontal distributions of ozone over Beijing from 2007 to 2010. Atmos Environ 74:37–44. doi:10.1016/j.atmosenv.2013.03.026

Chen YL, Feng JH (2001) Numerical simulations of airflow and cloud distributions over the windward side of the island of Hawaii. Part I: the effects of trade wind inversion. Mon Weather Rev 129:1117–1134. doi:10.1175/1520-0493(2001)129

Chen ZH, Cheng SY, Li JB, Guo XR, Wang WH, Chen DS (2008) Relationship between atmospheric pollution processes and synoptic pressure patterns in northern. China Atmos Environ 42:6078–6087. doi:10.1016/j.atmosenv.2008.03.043

Colle BA (2015) Mountain meteorology|Cold air damming. In: Zhang GRNP (ed) Encyclopedia of atmospheric sciences. Academic Press, Oxford, pp 62–68. doi:10.1016/B978-0-12-382225-3.00117-1

Colle BA, Smull BF, Yang MJ (2002) Numerical simulations of a landfalling cold front observed during COAST: rapid evolution and responsible mechanisms. Mon Weather Rev 130:1945–1966. doi:10.1175/1520-0493(2002)130

Cui ZQ, Tjernstrom M, Grisogono B (1998) Idealized simulations of atmospheric coastal flow along the central coast of California. J Appl Meteorol 37:1332–1363. doi:10.1175/1520-0450(1998)037
De Wekker SFJ (2008) Observational and numerical evidence of depressed convective boundary layer heights near a mountain base. J Appl Meteorol Clim 47:1017–1026. doi:10.1175/2007jamc1651.1
De Wekker SFJ, Kossmann M (2015) Convective boundary layer heights over mountainous terrain—a review of concepts. Front Earth Sci 3:77. doi:10.3389/feart.2015.00077
Ding AJ, Wang T, Thouret V, Cammas JP, Nedelec P (2008) Tropospheric ozone climatology over Beijing: analysis of aircraft data from the MOZAIC program. Atmos Chem Phys 8:1–13
Doyle JD (1997) The influence of mesoscale orography on a coastal jet and rainband. Mon Weather Rev 125:1465–1488. doi:10.1175/1520-0493(1997)125
Emery BR, Montague DC, Field RA, Parish TR (2015) Barrier wind formation in the upper green river basin of Sublette County. Wyoming, and its relationship to elevated ozone distributions in winter. J Appl Meteorol Clim 54:2427–2442. doi:10.1175/jamc-d-15-0103.1
Feng X, Li Q, Zhu YJ, Wang JJ, Liang HM, Xu RF (2014) Formation and dominant factors of haze pollution over Beijing and its peripheral areas in winter. Atmos Pollut Res 5:528–538. doi:10.5094/Apr.2014.062
Fu GQ, Xu WY, Yang RF, Li JB, Zhao CS (2014) The distribution and trends of fog and haze in the North China Plain over the past 30 years. Atmos Chem Phys 14:11949–11958. doi:10.5194/acp-14-11949-2014
Gao Y, Liu X, Zhao C, Zhang M (2011) Emission controls versus meteorological conditions in determining aerosol concentrations in Beijing during the 2008 Olympic Games. Atmos Chem Phys 11:12437–12451. doi:10.5194/acp-11-12437-2011
Gottlieb S, Shu CW (1998) Total variation diminishing Runge–Kutta schemes. Math Comput 67:73–85. doi:10.1090/S0025-5718-98-00913-2
Grubisic V, Doyle JD, Kuettner J, Mobbs S, Smith RB, Whiteman CD, Dirks R, Czyzyk S, Cohn SA, Vosper S, Weissmann M, Haimov S, De Wekker SFJ, Pan LL, Chow FK (2008) The terrain-induced rotor experiment: a field campaign overview including observational highlights. Bull Am Meteorol Soc 89:1513–1533. doi:10.1175/2008bams2487.1
Han L, Cheng S, Zhuang G, Ning H, Wang H, Wei W, Zhao X (2015) The changes and long-range transport of PM2.5 in Beijing in the past decade. Atmos Environ. doi:10.1016/j.atmosenv.2015.03.013
Hao JM, Wang LT, Li L, Hu JN, Yu XC (2005) Air pollutants contribution and control strategies of energy-use related sources in Beijing. Sci China Ser D 48:138–146. doi:10.1360/Yd0403
Harden BE, Renfrew IA, Petersen GN (2011) A climatology of wintertime barrier winds off Southeast Greenland. J Clim 24:4701–4717. doi:10.1175/2011jcli4113.1
He KB, Yang FM, Ma YL, Zhang Q, Yao XH, Chan CK, Cadle S, Chan T, Mulawa P (2001) The characteristics of PM2.5 in Beijing, China. Atmos Environ 35:4959–4970. doi:10.1016/S1352-2310(01)00301-6
Hitzl DE, Chen YL, Nguyen HV (2014) Numerical simulations and observations of airflow through the 'Alenuihaha Channel, Hawaii. Mon Weather Rev 142:4696–4718. doi:10.1175/Mwr-D-13-00312.1
Holt TR (1996) Mesoscale forcing of a boundary layer jet along the California coast. J Geophys Res 101:4235–4254. doi:10.1029/95jd03231
Hu JL, Wang YG, Ying Q, Zhang HL (2014) Spatial and temporal variability of PM2.5 and PM10 over the North China Plain and the Yangtze River Delta, China. Atmos Environ 95:598–609. doi:10.1016/j.atmosenv.2014.07.019
Hu X-M, Xue M (2016) Influence of synoptic sea breeze fronts on the urban heat Island intensity in Dallas-Fort Worth, Texas. Mon Weather Rev. doi:10.1175/MWR-D-15-0201.1
Hu X-M, Xue M, Klein PM, Illston BG, Chen S (2016) Analysis of urban effects in Oklahoma City using a dense surface observing network. J Appl Meteorol Clim. doi:10.1175/JAMC-D-15-0206.1
Hu X-M, Liu S (2005) Numerical simulation of land surface process and atmosphere boundary layer structure over small hill underlying surface. J Appl Meterol Sci 16:13–23
Hu X-M, Ma ZQ, Lin WL, Zhang HL, Hu JL, Wang Y, Xu XB, Fuentes JD, Xue M (2014) Impact of the Loess Plateau on the atmospheric boundary layer structure and air quality in the North China Plain: a case study. Sci Total Environ 499:228–237. doi:10.1016/j.scitotenv.2014.08.053
Huang JP, Zhou CH, Lee XH, Bao YX, Zhao XY, Fung J, Richter A, Liu X, Zheng YQ (2013) The effects of rapid urbanization on the levels in tropospheric nitrogen dioxide and ozone over East China. Atmos Environ 77:558–567. doi:10.1016/j.atmosenv.2013.05.030
Huang RJ, Zhang YL, Bozzetti C, Ho KF, Cao JJ, Han YM, Daellenbach KR, Slowik JG, Platt SM, Canonaco F, Zotter P, Wolf R, Pieber SM, Bruns EA, Crippa M, Ciarelli G, Piazzalunga A, Schwikowski M, Abbaszade G, Schnelle-Kreis J, Zimmermann R, An ZS, Szidat S, Baltensperger U, El Haddad I, Prevot ASH (2014) High secondary aerosol contribution to particulate pollution during haze events in China. Nature 514:218–222. doi:10.1038/Nature13774

Jackson P, Mayr G, Vosper S (2013) Dynamically-driven winds. In: Chow FK, de Wekker SFJ, Snyder BJ (eds) Mountain weather research and forecasting. Springer atmospheric sciences. Springer, Dordrecht, pp 121–218. doi:10.1007/978-94-007-4098-3

Ji DS, Li L, Wang YS, Zhang JK, Cheng MT, Sun Y, Liu ZR, Wang LL, Tang GQ, Hu B, Chao N, Wen TX, Miao HY (2014) The heaviest particulate air-pollution episodes occurred in northern China in January, 2013: insights gained from observation. Atmos Environ 92:546–556. doi:10.1016/j.atmosenv.2014.04.048

Jiang C, Wang H, Zhao T, Li T, Che H (2015) Modeling study of PM2.5 pollutant transport across cities in China's Jing-Jin-Ji region during a severe haze episode in December 2013. Atmos Chem Phys 15:5803–5814. doi:10.5194/acp-15-5803-2015

Lang JL, Cheng SY, Li JB, Chen DS, Zhou Y, Wei X, Han LH, Wang HY (2013) A monitoring and modeling study to investigate regional transport and characteristics of PM2.5 pollution. Aerosol Air Qual Res 13:943–956. doi:10.4209/aaqr.2012.09.0242

Lee JG, Xue M (2013) A study on a snowband associated with a coastal front and cold-air damming event of 3–4 February 1998 along the eastern coast of the Korean. Penins Adv Atmos Sci 30:263–279. doi:10.1007/s00376-012-2088-6

Li J, Chen YL (1998) Barrier jets during TAMEX. Mon Weather Rev 126:959–971. doi:10.1175/1520-0493(1998)126

Li XL, Shen XS, Peng XD, Xiao F, Zhuang ZR, Chen CG (2013) An accurate multimoment constrained finite volume transport model on Yin-Yang grids. Adv Atmos Sci 30:1320–1330. doi:10.1007/s00376-013-2217-x

Lin W, Xu X, Zhang X, Tang J (2008) Contributions of pollutants from north china plain to surface ozone at the shangdianzi GAW station. Atmos Chem Phys 8:5889–5898

Lindzen RS, Nigam S (1987) On the role of sea-surface temperature-gradients in Forcing low-level winds and convergence in the tropics. J Atmos Sci 44:2418–2436. doi:10.1175/1520-0469(1987)044

Loescher KA, Young GS, Colle BA, Winstead NS (2006) Climatology of barrier jets along the Alaskan coast. Part 1: spatial and temporal distributions. Mon Weather Rev 134:437–453. doi:10.1175/Mwr3037.1

Ma JZ, Wang W, Chen Y, Liu HJ, Yan P, Ding GA, Wang ML, Sun J, Lelieveld J (2012) The IPAC-NC field campaign: a pollution and oxidization pool in the lower atmosphere over Huabei, China. Atmos Chem Phys 12:3883–3908. doi:10.5194/acp-12-3883-2012

Ma JZ, Xu XB, Zhao CS, Yan P (2012b) A review of atmospheric chemistry research in China: photochemical smog, haze pollution, and gas-aerosol interactions. Adv Atmos Sci 29:1006–1026. doi:10.1007/s00376-012-1188-7

Malkus JS (1955) The effects of a large Island upon the trade-wind air stream. Q J R Meteorol Soc 81:538–550. doi:10.1002/qj.49708135003

Mao Y-H, Liao H, Han Y, Cao J (2016) Impacts of meteorological parameters and emissions on decadal and interannual variations of black carbon in China for 1980–2010. J Geophys Res 121:1822–1843. doi:10.1002/2015JD024019

McCauley MP, Sturman AP (1999) A study of orographic blocking and barrier wind development upstream of the Southern Alps, New Zealand. Meteorol Atmos Phys 70:121–131. doi:10.1007/s007030050029

Meng ZY, Xu XB, Yan P, Ding GA, Tang J, Lin WL, Xu XD, Wang SF (2009) Characteristics of trace gaseous pollutants at a regional background station in Northern China. Atmos Chem Phys 9:927–936

Miao Y, Hu X-M, Liu S, Qian T, Xue M, Zheng Y, Wang S (2015) Seasonal variation of local atmospheric circulations and boundary layer structure in the Beijing-Tianjin-Hebei region and implications for air quality. J Adv Model Earth Syst 7:1602–1626. doi:10.1002/2015ms000522

Nielsen ER, Schumacher RS, Keclik AM (2016) The effect of the Balcones Escarpment on three cases of extreme precipitation in Central Texas. Mon Weather Rev 144:119–138. doi:10.1175/MWR-D-15-0156.1

Olson JB, Colle BA (2009) Three-dimensional idealized simulations of barrier jets along the Southeast Coast of Alaska. Mon Weather Rev 137:391–413. doi:10.1175/2008mwr2480.1

Olson JB, Colle BA, Bond NA, Winstead N (2007) A comparison of two coastal barrier jet events along the southeast Alaskan coast during the SARJET field experiment. Mon Weather Rev 135:2973–2994. doi:10.1175/Mwr3448.1

Overland JE, Bond N (1993) The influence of coastal orography—the Yakutat Storm. Mon Weather Rev 121:1388–1397. doi:10.1175/1520-0493(1993)121

Overland JE, Bond N (1995) Observations and scale analysis of coastal wind jets. Mon Weather Rev 123:2934–2941. doi:10.1175/1520-0493(1995)123

Parish TR (1982) Barrier winds along the Sierra-Nevada mountains. J Appl Meteorol 21:925–930. doi:10.1175/1520-0450(1982)021

Parish TR (1983) The influence of the Antarctic Peninsula on the wind-field over the Western Weddell Sea. J Geophys Res 88:2684–2692. doi:10.1029/Jc088ic04p02684

Petersen GN, Renfrew IA, Moore GWK (2009) An overview of barrier winds off Southeastern Greenland during the Greenland flow distortion experiment. Q J R Meteorol Soc 135:1950–1967. doi:10.1002/qj.455

Pierrehumbert RT, Wyman B (1985) Upstream effects of mesoscale mountains. J Atmos Sci 42:977–1003. doi:10.1175/1520-0469(1985)042

Pu B, Dickinson RE (2014) Diurnal spatial variability of great plains summer precipitation related to the dynamics of the low-level jet. J Atmos Sci 71:1807–1817. doi:10.1175/JAS-D-13-0243.1

Qu WJ, Arimoto R, Zhang XY, Zhao CH, Wang YQ, Sheng LF, Fu G (2010) Spatial distribution and interannual variation of surface PM10 concentrations over eighty-six Chinese cities. Atmos Chem Phys 10:5641–5662. doi:10.5194/acp-10-5641-2010

Quan J, Zhang Q, He H, Liu J, Huang M, Jin H (2011) Analysis of the formation of fog and haze in North China Plain (NCP). Atmos Chem Phys 11:8205–8214. doi:10.5194/acp-11-8205-2011

Quan JN, Tie XX, Zhang Q, Liu Q, Li X, Gao Y, Zhao DL (2014) Characteristics of heavy aerosol pollution during the 2012–2013 winter in Beijing, China. Atmos Environ 88:83–89. doi:10.1016/j.atmosenv.2014.01.058

Rendon AM, Salazar JF, Palacio CA, Wirth V (2015) Temperature inversion breakup with impacts on air quality in urban valleys influenced by topographic shading. J Appl Meteorol Clim 54:302–321. doi:10.1175/Jamc-D-14-0111.1

Rotunno R, Ferretti R (2001) Mechanisms of intense alpine rainfall. J Atmos Sci 58:1732–1749. doi:10.1175/1520-0469(2001)058

Saide PE, Carmichael GR, Spak SN, Gallardo L, Osses AE, Mena-Carrasco MA, Pagowski M (2011) Forecasting urban PM10 and PM2.5 pollution episodes in very stable nocturnal conditions and complex terrain using WRF-Chem CO tracer model. Atmos Environ 45:2769–2780. doi:10.1016/j.atmosenv.2011.02.001

Schnadt H, Ivanov I (2012) Chapter 7—environmental consequences and management of a severe accident. In: Sehgal BR (ed) Nuclear safety in light water reactors. Academic Press, Boston, pp 589–624. doi:10.1016/B978-0-12-388446-6.00007-1

Schwerdtfeger W (1975) Effect of Antarctic Peninsula on temperature regime of Weddell Sea. Mon Weather Rev 103:45–51. doi:10.1175/1520-0493(1975)103

Schwerdtfeger W (1979) Meteorological aspects of the drift of ice from the Weddell Sea toward the Mid-Latitude westerlies. J Geophys Res 84:6321–6328. doi:10.1029/Jc084ic10p06321

Sheridan PF, Horlacher V, Rooney GG, Hignett P, Mobbs SD, Vosper SB (2007) Influence of lee waves on the near-surface flow downwind of the Pennines. Q J R Meteorol Soc 133:1353–1369. doi:10.1002/Qj.110

Smith RB (1982) Synoptic observations and theory of orographically disturbed wind and pressure. J Atmos Sci 39:60–70. doi:10.1175/1520-0469(1982)039

Steyn D, De Wekker SJ, Kossmann M, Martilli A (2013) Boundary layers and air quality in mountainous terrain. In: Chow FK, De Wekker SFJ, Snyder BJ (eds) Mountain weather research and forecasting. Springer atmospheric sciences. Springer, Berlin, pp 261–289. doi:10.1007/978-94-007-4098-3-5

Stull RB (1988) An introduction to boundary layer meteorology. Springer, Dordrecht, 666 pp

Sun YL, Zhuang GS, Tang AH, Wang Y, An ZS (2006) Chemical characteristics of PM2.5 and PM10 in haze-fog episodes in Beijing. Environ Sci Technol 40:3148–3155. doi:10.1021/Es051533g

van Donkelaar A, Martin RV, Brauer M, Kahn R, Levy R, Verduzco C, Villeneuve PJ (2010) Global estimates of ambient fine particulate matter concentrations from satellite-based aerosol optical depth: development and application. Environ Health Persp 118:847–855. doi:10.1289/Ehp.0901623

Vosper SB, Sheridan PF, Brown AR (2006) Flow separation and rotor formation beneath two-dimensional trapped lee waves. Q J R Meteorol Soc 132:2415–2438. doi:10.1256/Qj.05.174

Wang F, Chen DS, Cheng SY, Li JB, Li MJ, Ren ZH (2010) Identification of regional atmospheric PM10 transport pathways using HYSPLIT, MM5-CMAQ and synoptic pressure pattern analysis. Environ Model Softw 25:927–934. doi:10.1016/j.envsoft.2010.02.004

Wang L, Zhang N, Liu Z, Sun Y, Ji D, Wang Y (2014) The Influence of climate factors, meteorological conditions, and boundary-layer structure on severe haze pollution in the Beijing-Tianjin-Hebei region during January 2013. Adv Meteorol 2014:14. doi:10.1155/2014/685971

Wang T, Nie W, Gao J, Xue LK, Gao XM, Wang XF, Qiu J, Poon CN, Meinardi S, Blake D, Wang SL, Ding AJ, Chai FH, Zhang QZ, Wang WX (2010) Air quality during the 2008 Beijing Olympics: secondary pollutants and regional impact. Atmos Chem Phys 10:7603–7615. doi:10.5194/acp-10-7603-2010

Wang Y, Ying Q, Hu J, Zhang H (2014) Spatial and temporal variations of six criteria air pollutants in 31 provincial capital cities in China during 2013–2014. Environ Int 73:413–422. doi:10.1016/j.envint.2014.08.016

Wang ZB, Hu M, Wu ZJ, Yue DL, He LY, Huang XF, Liu XG, Wiedensohler A (2013) Long-term measurements of particle number size distributions and the relationships with air mass history and source apportionment in the summer of Beijing. Atmos Chem Phys 13:10159–10170. doi:10.5194/acp-13-10159-2013

Wei P, Cheng SY, Li JB, Su FQ (2011) Impact of boundary-layer anticyclonic weather system on regional air quality. Atmos Environ 45:2453–2463. doi:10.1016/j.atmosenv.2011.01.045

Wei P, Ren Z, Su F, Cheng S, Zhang P, Gao Q (2011b) Environmental process and convergence belt of atmospheric NO_2 pollution in North China. Acta Meteorol Sin 25:797–811. doi:10.1007/s13351-011-0610-x

Whiteman CD (2000) Mountain meteorology: fundamentals and applications: fundamentals and applications. Oxford University Press, Oxford

Whiteman CD, Doran JC (1993) The relationship between overlying synoptic-scale flows and winds within a valley. J Appl Meteorol 32:1669–1682. doi:10.1175/1520-0450(1993)032

Wu D, Liao BT, Wu M, Chen H, Wang Y, Niao X, Gu Y, Zhang X, Zhao XJ, Quan JN, Liu WD, Meng J, Sun D (2014) The long-term trend of haze and fog days and the surface layer transport conditions under haze weather in North China. Acta Sci Circumst 34:1–11

Wu ZJ, Hu M, Lin P, Liu S, Wehner B, Wiedensohler A (2008) Particle number size distribution in the urban atmosphere of Beijing, China. Atmos Environ 42:7967–7980. doi:10.1016/j.atmosenv.2008.06.022

Xu J, Ma JZ, Zhang XL, Xu XB, Xu XF, Lin WL, Wang Y, Meng W, Ma ZQ (2011) Measurements of ozone and its precursors in Beijing during summertime: impact of urban plumes on ozone pollution in downwind rural areas. Atmos Chem Phys 11:12241–12252. doi:10.5194/acp-11-12241-2011

Xu Q (1990) A theoretical-study of cold air damming. J Atmos Sci 47:2969–2985. doi:10.1175/1520-0469(1990)047

Xu WY, Zhao CS, Ran L, Deng ZZ, Liu PF, Ma N, Lin WL, Xu XB, Yan P, He X, Yu J, Liang WD, Chen LL (2011) Characteristics of pollutants and their correlation to meteorological conditions at a suburban site in the North China Plain. Atmos Chem Phys 11:4353–4369. doi:10.5194/acp-11-4353-2011

Xu X, Wang Y, Zhao T, Cheng X, Meng Y, Ding G (2015) “Harbor” effect of large topography on haze distribution in eastern China and its climate modulation on decadal variations in haze. Chin Sci Bull 60:1132–1143. doi:10.1360/n972014-00101

Xue M, Lin SJ (2001) Numerical equivalence of advection in flux and advective forms and quadratically conservative high-order advection schemes. Mon Weather Rev 129:561–565. doi:10.1175/1520-0493(2001)129

Yang L, Wu Y, Davis JM, Hao JM (2011) Estimating the effects of meteorology on PM2.5 reduction during the 2008 summer Olympic Games in Beijing, China. Front Environ Sci Eng China 5:331–341. doi:10.1007/s11783-011-0307-5

Yang Y, Chen YL (2008) Effects of terrain heights and sizes on island-scale circulations and rainfall for the island of Hawaii during HaRP. Mon Weather Rev 136:120–146. doi:10.1175/2007mwr1984.1

Ye X, Song Y, Cai X, Zhang H (2015) Study on the synoptic flow patterns and boundary layer process of the severe haze events over the North China Plain in January 2013. Atmos Environ 124:129–145. doi:10.1016/j.atmosenv.2015.06.011

Zhang H, Wang Y, Hu J, Ying Q, Hu X-M (2015) Relationships between meteorological parameters and criteria air pollutants in three megacities in China. Environ Res 140:242–254. doi:10.1016/j.envres.2015.04.004

Zhang JP, Zhu T, Zhang QH, Li CC, Shu HL, Ying Y, Dai ZP, Wang X, Liu XY, Liang AM, Shen HX, Yi BQ (2012) The impact of circulation patterns on regional transport pathways and air quality over Beijing and its surroundings. Atmos Chem Phys 12:5031–5053. doi:10.5194/acp-12-5031-2012

Zhang Q, Ma XC, Tie XX, Huang MY, Zhao CS (2009) Vertical distributions of aerosols under different weather conditions: analysis of in-situ aircraft measurements in Beijing, China. Atmos Environ 43:5526–5535. doi:10.1016/j.atmosenv.2009.05.037

Zhang RH, Li Q, Zhang RN (2014) Meteorological conditions for the persistent severe fog and haze event over eastern China in January 2013. Sci China Earth Sci 57:26–35. doi:10.1007/s11430-013-4774-3

Zhang XY, Wang YQ, Lin WL, Zhang YM, Zhang XC, Gong S, Zhao P, Yang YQ, Wang JZ, Hou Q, Zhang XL, Che HZ, Guo JP, Li Y (2009b) Changes of atmospheric composition and optical properties over Beijing 2008 Olympic monitoring campaign. Bull Am Meteorol Soc 90:1633–1651. doi:10.1175/2009bams2804.1

Zhang XY, Wang YQ, Niu T, Zhang XC, Gong SL, Zhang YM, Sun JY (2012) Atmospheric aerosol compositions in China: spatial/temporal variability, chemical signature, regional haze distribution and comparisons with global aerosols. Atmos Chem Phys 12:779–799. doi:10.5194/acp-12-779-2012

Zhang Z, Zhang X, Gong D, Quan W, Zhao X, Ma Z, Kim S-J (2015) Evolution of surface O_3 and $PM_2.5$ concentrations and their relationships with meteorological conditions over the last decade in Beijing. Atmos Environ 108:67–75. doi:10.1016/j.atmosenv.2015.02.071

Zhao PS, Dong F, He D, Zhao XJ, Zhang XL, Zhang WZ, Yao Q, Liu HY (2013) Characteristics of concentrations and chemical compositions for $PM_2.5$ in the region of Beijing, Tianjin, and Hebei, China. Atmos Chem Phys 13:4631–4644. doi:10.5194/acp-13-4631-2013

Zhao XJ, Zhao PS, Xu J, Meng W, Pu WW, Dong F, He D, Shi QF (2013) Analysis of a winter regional haze event and its formation mechanism in the North China Plain. Atmos Chem Phys 13:5685–5696. doi:10.5194/acp-13-5685-2013